Elastic scattering of π^+ and π^- from ^{40}Ca at 64.8 MeV

S. H. Dam,* R. D. Edge, and B. M. Preedom
University of South Carolina, Columbia, South Carolina 29208

M. Hamm, R. L. Burman, R. Carlini, R. P. Redwine,† and M. A. Yates
Los Alamos National Laboratory, Los Alamos, New Mexico 87545

M. Blecher and K. Gotow
Virginia Polytechnic Institute and State University, Blacksburg, Virginia 24061

F. E. Bertrand and E. E. Gross
Oak Ridge National Laboratory, Oak Ridge, Tennessee 37830

M. A. Moinester
Tel Aviv University, Ramat Aviv, Israel

(Received 27 July 1981; revised manuscript received 2 February 1982)

Angular distributions of π^+ and π^- elastic scattering on ^{40}Ca at 64.8 MeV are presented. The data are analyzed using a first-order, nonlocal optical model based on a Kisslinger t matrix with an off-shell form factor. This model is unable to fit the data for any value of the off-shell parameter α unless the nuclear matter radius is allowed to vary from that derived from electron scattering. The resulting best-fit radii are as much as 0.40 fm larger than the electron scattering value for π^+ and 0.55 fm larger for π^-. For a given α the π^- best fit radius is also consistently larger by about 0.2 fm than that for π^+. In addition, the fits show no significant preference for any value of α between 400 and 900 MeV/c. Inclusion of the normally omitted second-order potential terms in the optical model does not significantly alter the results.

[NUCLEAR REACTIONS π^+ and π^- elastic scattering from ^{40}Ca at 64.8 MeV; angular distributions, $15° < \theta_{lab} < 127°$; optical model analysis.]

I. INTRODUCTION

Pion-nuclear physics is an important application of many body theory to a fairly simple strongly interacting system. Since the pion is spinless, many of the complicated spin-dependent effects present in the nucleon-nucleus interaction play no role. However, the basis pion-nucleon (πN) interaction, while very weak at low energy, becomes resonant at a pion energy of around 185 MeV. In pion-nucleus scattering this energy dependence is reflected in the interaction being primarily at the surface near the resonance energy, while at lower energies pions more easily penetrate to the nuclear interior. The present collaboration has concentrated on the low energy region of pion-nucleus interactions and has recently published several studies[1–4] of π^+ elastic scattering from various targets at energies from 30 to 50 MeV. These and other experiments have also been summarized in recent reviews.[5,6]

The energy region between 50 and 100 MeV is of particular interest since it represents a transition from a weak to a strongly resonant interaction in the pion-nucleus system. However, the experimental data in this region are quite sparse. As the first in a series of π^+ and π^- elastic scattering studies in this energy region, this paper presents the results for π^+ and π^- scattering from ^{40}Ca at 64.8 MeV. Also presented are attempts to fit these data with a first-order phenomenological optical model.

The measurement of both π^+ and π^- distributions is important for several reasons. Cross sections for single charge exchange can be predicted from π^+ and π^- elastic scattering cross sections,[7] and a comparison of these for $N=Z$ targets may lead to information about the off-shell behavior of the πN interaction.[8] Also, data from scattering both charged pions in this region should provide a stringent test of pion-nucleus scattering theories,

particularly with regard to the correct treatment of the Coulomb part of the interaction.

II. EXPERIMENTAL PROCEDURE

The data were taken using the Bicentennial Spectrometer at the low energy pion (LEP) channel[9] of the Clinton P. Anderson Los Alamos Meson Physics Facility (LAMPF). This spectrometer is a double focusing, broad range device originally used at the Florida State University tandem van de Graff facility.[10] It was rebuilt at LAMPF with the installation of new coils and an increase in the pole gap from 2.5 to 5 cm in order to increase the effective solid angle. The path length of the central ray through the spectrometer is only 2 m, which minimizes the amount of pion decay. Other design characteristics are as follows: angular acceptance, $\pm 2°$ azimuthal and $\pm 2.8°$ scattering angle; solid angle, 6 msr at full acceptance; momentum resolution, 0.2 to 0.3 % FWHM; momentum range, p_0 to 1.5 p_0; maximum momentum, 180 MeV/c at 10 kG. Owing to the finite beam spot from the LEP channel, the effective solid angle of the spectrometer changes with the scattering angle. This variation was carefully measured by changing the magnetic field of the spectrometer in small steps, and recording elastic scattering from a ^{12}C target at each setting. The area of the elastic peak was then divided by the beam monitor counts (to be described below) and least-squares fitted in sections in order to obtain an analytic description of the distribution to be used in cross section determinations. Figure 1 shows this solid angle distribution normalized to one in the flat region as a function of the focal plane position of the elastic peak.

The detector array is schematically shown in Fig. 2. Scattered pions are momentum analyzed by the spectrometer and are detected by a helical wire chamber[11] placed at the focal plane. A second wire chamber placed above the first provides angle information used to reduce background. The event signature is defined by a coincidence between a small scintillator ($S0$) placed between the target and the x-y collimating slits, a large scintillator ($S1$) mounted after the second wire chamber, and a y-axis (perpendicular to the bend plane of the magnet) signal from either wire chamber. This trigger provides an extremely clean event signature.

The operating conditions of the LEP channel were as follows: solid angle, 17.6 msr; beam energy at the center of the target, 64.8 MeV; momentum bite ($\delta p/p$), $\pm 0.4\%$ for scattering angles $< 30°$ and $\pm 0.75\%$ for all other angles. The smaller momentum bite at small angles was used to reduce the dead time in the focal plane detectors.

The relative normalization of the incident beam flux was accomplished using a pion decay monitor.[12] Two scintillators (π-$\mu 1$ and π-$\mu 2$ in Fig. 1) placed at an angle of 7° from the beam were used to detect muons from decaying beam pions. This angle falls within a relatively constant region in the phase-space Jacobian of the pion to muon decay. The position and size of the π-μ scintillators were designed to sample most of the horizontal cross section of the beam, so that small fluctuations about the beam centerline produced no appreciable changes in the relative normalization. The pion decay monitor was checked against the primary proton beam monitor and was found to be stable within statistical uncertainties of $\pm 2\%$.

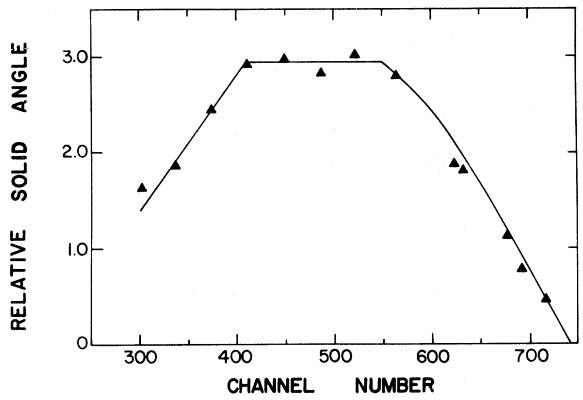

FIG. 1. Relative solid angle as a function of focal plane position for the Bicentennial Spectrometer. The solid line is a least-squares fit to the data.

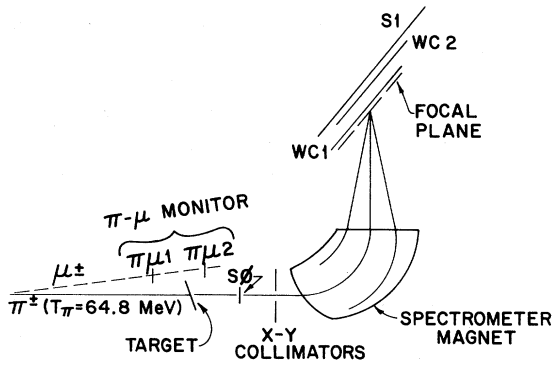

SCHEMATIC OF EXPERIMENTAL APPARATUS

FIG. 2. Schematic diagram of spectrometer setup.

The absolute normalization was determined by measuring the π^+-p cross section at laboratory angles of 55°, 93°, and 113°, and suitably normalizing to the data of Bertin *et al.*[13] This normalizes the π-μ monitor to the product of beam flux and spectrometer acceptance. The uncertainty in this absolute normalization was $\pm 5\%$ for the π^+ data. In the absence of data for π^--p at 65 MeV, the same calibration of the π-μ relative monitor was used as for π^+ while increasing the uncertainty to 7% in order to account for any possible change in the beam geometry between π^+ and π^-.

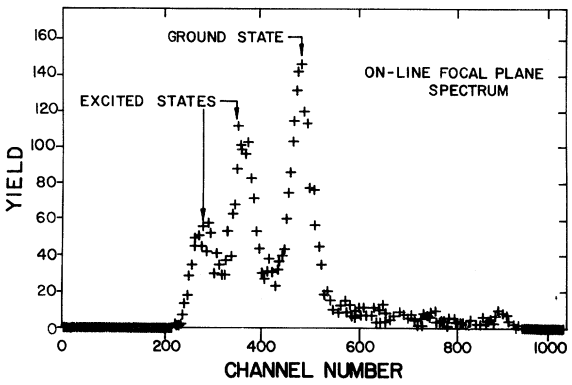

FIG. 3. Representative on-line focal plane spectrum taken at $\theta_{lab} = 100°$.

III. DATA REDUCTION

As with most experiments involving calcium targets, the presence of CaO was of some concern. The thickness of the oxide layer was measured several months after the experiment was performed by an electron microprobe (an electron backscattering technique) and was found to be approximately 15 mg/cm^2 of oxygen out of a total target thickness of 339.6 mg/cm^2. Owing to the uncertainty in the actual amount of oxygen present in the target during the experiment and the lack of measured $\pi^{\pm}$-^{16}O cross sections at 65 MeV, the absolute error bars on the $\pi^{\pm}$-^{40}Ca data were increased by an amount equal to calculated $\pi^{\pm}$-^{16}O cross sections using interpolated optical model parameters and assuming an oxygen contamination of half the measured value. This amount of oxygen was considered a reasonable estimate based on the observed spectral shapes in the diffraction minimum region of the angular distribution, where pion scattered from the contamination will be an appreciable part of the yield.

Other contaminants in the elastic peak resulted from the detection of scattered muons from the beam and protons from pion absorption in the target. Protons were eliminated from the LEP beam using degraders, and scattered electrons were eliminated by a pulse height threshold setting in the scintillator electronics. Owing to the selectivity of the hardware event trigger, there was very little background in the on-line focal plane spectra. Figure 3 shows a representative spectrum to which only multiple-event and overflow software cuts have been applied. Other cuts were applied in the off-line analysis, such as scintillator pulse height tests and cuts based on the angle of incidence of the event on the wire chambers, but these were found to have a relatively small effect (2%) on the peak area above background, and served mainly to eliminate events due to pion absorption in the target. The contribution due to scattered muons was subtracted via the calculated Coulomb cross section, assuming previously measured ratios for μ's to π's of 0.13 for π^+ and 0.11 for π^- at 65 MeV. This correction is most important at the forward angles.

Even though the cross sections were normalized to known π^+-p scattering at 65 MeV, a small correction was necessary to account for the difference in the amount of pion decay through the apparatus owing to the different kinematics for π-p vs π-Ca elastic scattering at the various calibration angles. This correction amounted to an overall 7% decrease in the absolute cross sections. Further corrections to the data were made for the finite solid angle of the spectrometer system and finite size of the beam at the target. These corrections are appreciable in regions of the angular distribution where the cross section changes rapidly and nonlinearly as a function of the scattering angle.

The absolute cross sections, obtained by applying all the above described corrections, folding in the relative solid angle acceptance of the spectrometer, and normalizing to π-p cross sections, are tabulated in Table I and plotted in Fig. 4. Three distinct phenomena are apparent in these spectra: (1) the Coulomb-nuclear interference at small angles; (2) a shoulder around 60° in the center of mass due to the so-called s-p wave interference; and (3) the first diffraction minimum at around 100° with the π^- at a slightly smaller angle due to Coulomb effects. The forward angle regions have different shapes and magnitudes since the interference between Coulomb and nuclear scattering is constructive for π^- and destructive for π^+. The other major difference is the stronger s-p minimum for the π^+ scattering due to the enhancement of the s-wave repulsion by the

TABLE I. Absolute differential cross sections for $\pi^{\pm}$-^{40}Ca elastic scattering at T_π=64.8 MeV.

$\theta_{c.m.}$	$(d\sigma/d\Omega)\pi^+$ (mb/sr)	$(d\sigma/d\Omega)\pi^-$ (mb/sr)
15.4		1409.0 ±62.0
20.4	143.0 ±9.0	830.0 ±34.0
25.4	121.0 ±5.0	501.0 ±21.0
30.5	98.6 ±4.5	279.0 ±11.0
35.5	69.0 ±3.0	142.0 ± 7.0
40.5	45.2 ±2.1	80.4 ± 4.3
45.5	25.4 ±1.2	47.4 ± 2.7
50.5	13.9 ±0.7	24.4 ± 1.4
55.6	7.32±0.43	21.1 ± 1.3
60.6	6.59±0.39	18.1 ± 1.1
65.6	6.58±0.30	17.7 ± 0.9
70.6	6.93±0.30	15.5 ± 0.9
75.6	5.69±0.27	11.5 ± 0.7
80.6	4.87±0.29	5.30± 0.37
85.6	2.88±0.24	3.04± 0.27
90.6	2.08±0.21	1.19± 0.22
95.6	0.80±0.21	0.41± 0.20
100.6	0.51±0.19	0.54± 0.18
103.1	0.59±0.18	
105.6	0.72±0.17	0.98± 0.15
115.0	1.66±0.13	
120.0	1.80±0.13	2.41± 0.14
125.0	2.99±0.13	
128.0	2.81±0.13	1.99± 0.10

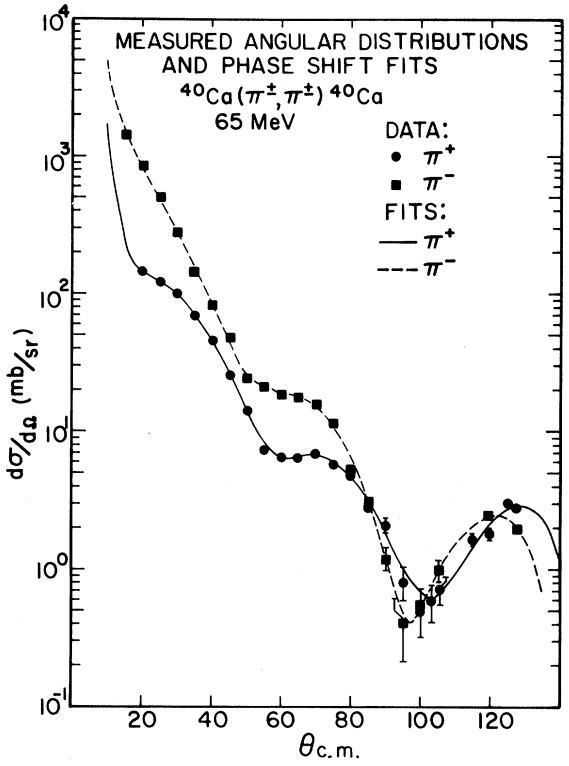

FIG. 4. Measured $\pi^{\pm}$-^{40}Ca angular distributions with phase shift fits. The number of partial waves used was 6 for π^+ and 5 for π^-, producing a χ^2/N of 2.1 and 2.0, respectively.

Coulomb repulsion.

The curves drawn in Fig. 4 are phase shift fits to the data. The chi-squared value (χ^2) per degree of freedom is 2.1 for π^+ and 2.0 for π^-.

IV. OPTICAL MODEL ANALYSIS

The amount of structure in the angular distributions presented here should provide a stringent test for a first order optical model of pion-nucleus scattering. An extensive study of such a model's ability to fit these data has been performed using a coordinate space code developed by Gibbs, Gibson, and Stephenson.[14] This code utilizes a phenomenological, nonlocal, Kisslinger t matrix which in momentum space notation can be written as follows:

$$t(q,q',E) \propto \frac{(k^2+\alpha^2)^2}{(\alpha^2+q^2)(\alpha^2+q'^2)} \times[b_0 k^2 + b_1(\vec{q}\cdot\vec{q}')] \,. \quad (1)$$

In this expression, α is an off-shell parameter describing a vertex nonlocality in the pion-nucleon interaction, k and E are the on-shell pion momentum and energy, $\vec{q}$ and $\vec{q}'$ are the local pion-nucleon relative momenta before and after the interaction, and b_0 and b_1 are the complex s- and p-wave strength parameters. Since there is considerable evidence[15] indicating that strengths determined from free pion-nucleon phase shifts cannot adequately describe the low energy pion elastic scattering data, the strengths have been treated as free parameters in the present study.

The nuclear matter density is taken to be a Woods-Saxon distribution

$$\rho(r) = \frac{N(c,a)}{1+e^{(r-c)/a}} \,, \quad (2)$$

where $N(c,a)$ is the normalization, c is the half-density radius, and a is the diffuseness. The body geometry parameters c and a for ^{40}Ca were initially determined by choosing a set which, when convoluted with a proton charge radius of 0.81 fm, gave the

same rms radius as determined from electron scattering, and also reproduced the electron scattering form factor out to several minima.[16,17] The geometry for the matter distribution thus obtained was $c=3.63$ fm and $a=0.51$ fm, which differs slightly from the $c=3.68$ fm and $a=0.58$ fm used at lower energies.[4] However, both sets of geometry parameters give equally good fits to the lower energy data.

The initial attempts to fit the data were performed using the above geometry while searching internally on the strength parameters b_0 and b_1 for fixed values of the off-shell parameter α. One of the purposes of this study was to gain some quantitative information on the effective nonlocality of the elementary pion-nucleon interaction in nuclear matter by finding a value of α which would produce good fits to both the π^+ and π^- data. However, it was found that the model was unable to give reasonable fits to either set for any value of α with the geometry derived from electron scattering. The χ^2's per degree of freedom were greater than 10 for these cases. Representative "fits" for the case of $\alpha=500$ MeV/c and using the physical matter distribution are shown as the solid lines in Figs. 5 and 6.

The poor fits obtained with this geometry are presumably indicative of the need to include additional effects in the optical model, some of which can be mocked up by a change in the radius of the Woods-Saxon density distribution. Evidence that such a modification produces better fits to data in this energy region has previously been reported in analyses of 50 MeV π^+ scattering on ^{12}C and ^{16}O (Refs. 2 and 16, respectively).

Figure 7 presents a series of χ^2 distributions resulting from varying the radius parameter c for several values of α, while keeping the diffuseness fixed. In all cases, the strength parameters were internally varied to produce the best fit. It is obvious from these curves that by allowing the nuclear matter radius to vary, the first order optical model applied here can produce reasonable and in some cases excellent fits to these data. There are, however, obvious quantitative differences between the π^+ and π^- fits. Most obvious is the difference in the χ^2 of the best fit for each α. At every value of α tried, the model was able to fit the π^- data much better than the π^+, the difference being mainly in the inability to simultaneously reproduce the diffraction and s-p interference minima in the π^+ data. The other major difference is that for a given α, the radii at which the best fits occur are consistently about 0.2 to 0.3 fm larger for π^- than for π^+.

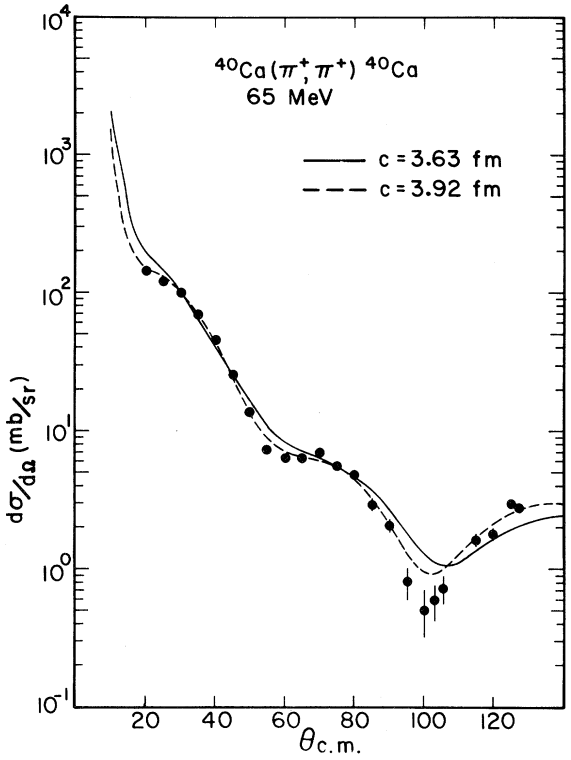

FIG. 5. Comparison of optical model fits to the π^+ data for electron scattering geometry (solid curve) and best-fit geometry (dashed curve) with an off-shell parameter α of 500 MeV/c, and fixed diffuseness, a of 0.51 fm. The corresponding χ^2/N of the fits are 14.9 and 3.5, respectively.

Even though there is no overwhelming preference for α between 400 and 900 MeV/c, the curves do show a slight preference for an α of 900 MeV/c in the π^- fits. Representative fits corresponding to $\alpha=500$ MeV/c are plotted in Figs. 5 and 6 as the dashed curves. The radii corresponding to these fits are 3.92 fm for π^+ and 4.12 fm for π^-. Note that even the π^+ radius is some 0.3 fm larger than the original 3.63 fm, a strong indication that higher order effects will play an important role in adequately describing these data. The difference between the π^- and π^+ radii, however, is disturbing and difficult to explain since the target is an $N=Z$ nucleus, and the coordinate space fitting code explicitly takes into account the Coulomb part of the interaction. Thus there should be no large charge-dependent effects, not even in higher order terms.

In the solution of the Klein-Gordon equation, the second-order potential terms, $V_N{}^2$ and $V_NV_C+V_CV_N$, are normally estimated to be small compared to V_N+V_C and hence are omitted. Since

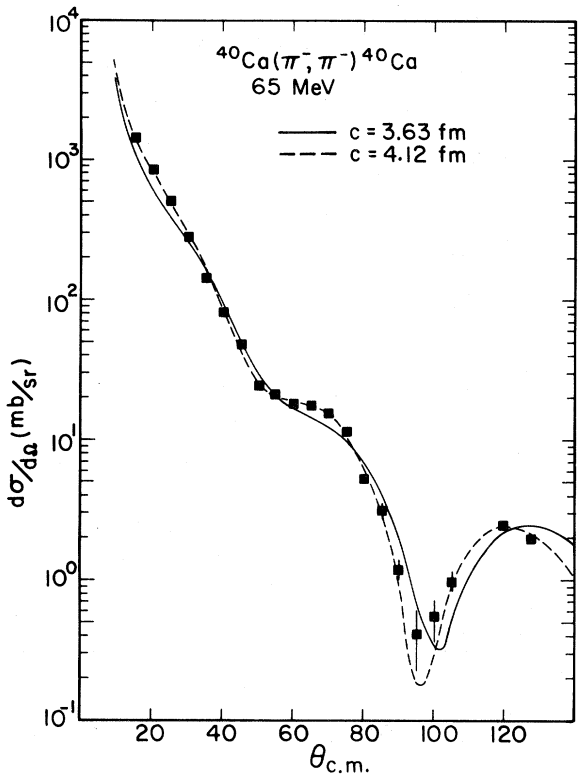

FIG. 6. Comparison of optical model fits to the π^- data for electron scattering geometry (solid curve) and best-fit geometry (dashed curve) with an off-shell parameter α of 500 MeV/c, and fixed diffuseness, a, of 0.51 fm. The corresonding χ^2/N of the fits are 13.6 and 1.5, respectively.

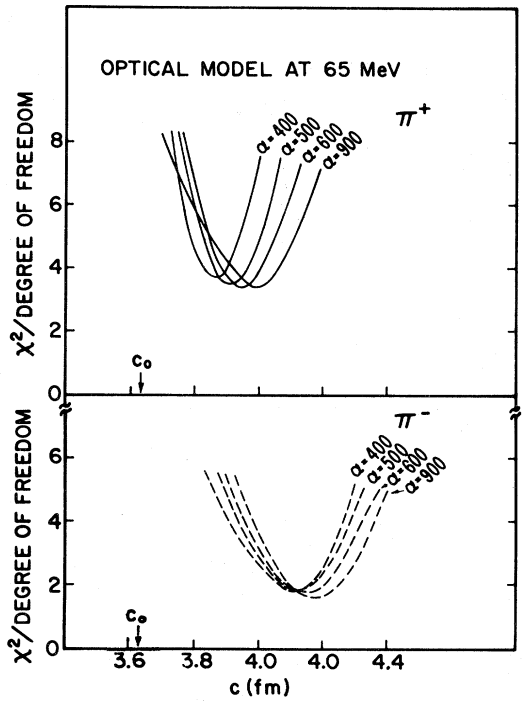

FIG. 7. Series of χ^2 distributions for the π^+ and π^- data as a function of the off shell and radius parameters, α and c, for the normal optical model. The radius derived from electron scattering is indicated by c_0.

the first term contributes ρ^2 terms from the first-order potential and the second term is charge dependent, the code was modified to include these terms in order to determine their effect on the best-fit geometry. Figure 8 shows representative α-c χ^2 distributions for the modified potential. Comparison of these with the curves of Fig. 7 shows that inclusion of the normally omitted terms changes the overall character of the fits as a function of the α and c parameters. The radii needed to fit the data are now smaller than in the previous cases, but still considerably larger than the value derived from electron scattering; however, the radius difference between π^+ and π^- persists. The π^+ and π^- curves now show a slight preference for an α of around 500 MeV/c. Figure 9 shows the fitted angular distributions corresponding to the representative case of $\alpha = 500$ MeV/c for the modified version of the model.

Table II is a tabulation of the fitted strength parameters for various α-c pairs along the loci of minima for both the normal and modified cases. For a given set of fits, there is little difference in the fitted strength parameters as a function of α, so that within the range indicated, the best-geometry fits can be considered essentially equivalent. The only exception is in the case of the normal fit to π^- at $\alpha = 400$ MeV/c, where the Reb_0 is anomalously large. The differences between the π^+ and π^- b_1 strength parameters for a given α can be qualitatively explained by the fact that the π^- interaction with nucleons in the nucleus is at an effectively higher energy than the π^+ due to the Coulomb interaction. Phase shift predictions show an increase of these parameters with energy in this region.[15,18] However, the Reb_0 and Imb_0 parameters are predicted to be fairly constant with energy, while the π^- fits produce values for these parameters that are considerably larger in absolute magnitude than those for π^+. In general, all the parameters are considerably larger in magnitude than the predictions. Since the fitted strength parameters are influenced by effects not explicitly included in the model, and the phase-shift derived strengths must be corrected for the presence of other nucleons, any quantitative comparision of the two is difficult.

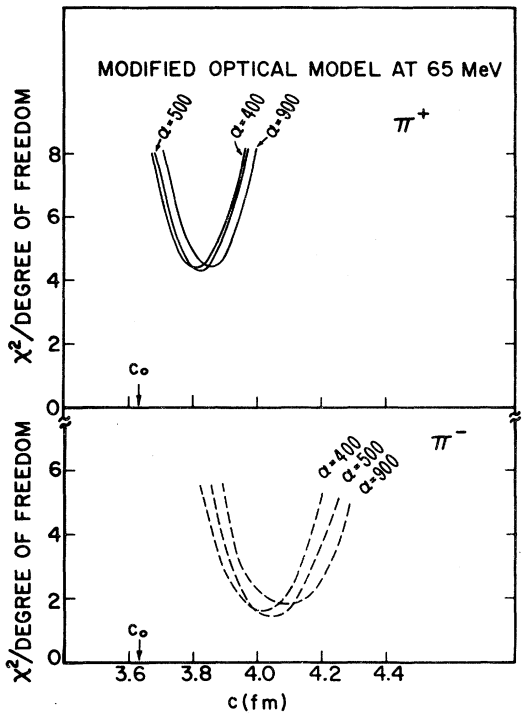

FIG. 8. Series of χ^2 distributions for the π^+ and π^- data as a function of the off shell and radius parameters, α and c, for the modified optical model (see text). The radius derived from electron scattering is indicated by c_0.

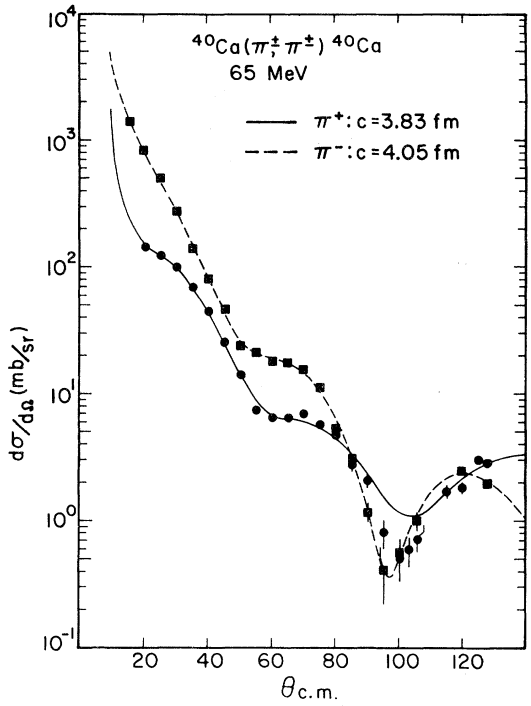

FIG. 9. Modified optical model fits (see text) to the π^+ and π^- data with an off-shell parameter $\alpha=500$ MeV/c and diffuseness $a=0.51$ fm, for best-fit radii as indicated. The corresponding χ^2/N are 4.3 for π^+ and 1.4 for π^-.

V. SUMMARY AND CONCLUSIONS

Neither the π^+ nor the π^- data presented here can be fitted with a phenomenological first-order optical model unless the nuclear matter geometry is allowed to vary from the geometry determined from electron scattering. Good fits to the π^- data, and reasonable fits to the π^+ data, can be obtained for

TABLE II. Results of normal and modified optical model best geometry fits for various values of α, the off-shell parameter. The diffuseness parameter, a, has been fixed at 0.51 fm.

Case	α MeV/c	c[a] fm	Reb_0 fm^3	Imb_0 fm^3	Reb_1 fm^3	Imb_1 fm^3	χ^2/N
π^+	400	3.87	−3.25	−0.98	7.04	2.38	3.7
	500	3.92	−3.20	−1.02	7.00	2.24	3.5
	900	4.00	−3.06	−1.07	6.81	1.96	3.4
π^+, modified[b]	400	3.82	−3.34	−0.94	7.02	2.60	4.3
	500	3.83	−3.31	−0.96	6.93	2.54	4.3
	900	3.85	−3.22	−1.00	6.68	2.44	4.4
π^-	400	4.12	−4.75	−3.46	8.29	3.99	1.8
	500	4.12	−2.81	−2.95	7.54	4.08	1.9
	900	4.18	−2.43	−2.60	6.83	3.27	1.6
π^-, modified[b]	400	4.02	−5.32	−4.32	9.27	5.51	1.6
	500	4.05	−5.32	−4.01	8.93	4.97	1.4
	900	4.10	−5.19	−3.62	8.33	4.36	1.8

[a]Best-fit radius.

[b]Code modified to include $V_N{}^2$ and $V_NV_C+V_CV_N$ terms (see text).

values of c, the Woods-Saxon radius parameter, that are considerably larger than that expected from electron scattering. This is not to be interpreted as a true reflection of the nuclear matter density, but rather as an indication of the need to include higher order terms in the model. The poorer fits for the π^+ data are apparently owing to the fact that the π^+ angular distribution exhibits more structure in the s-p interference region, making it more difficult for the model to simultaneously reproduce this region and the diffraction minimum.

For a given value of α, the off-shell parameter, the best fits to the two angular distributions occur at quite different radii, 0.2 to 0.3 fm different, a result difficult to explain. Nor is there any great preference exhibited by the fits for any particular α in the range of 400 to 900 MeV/c, making it impossible to gain any quantitative information about the off-shell behavior of the elementary interaction from this analysis.

Inclusion of the normally omitted $V_N{}^2$ and $V_N V_C + V_C V_N$ terms in the Klein-Gordon equation does not succeed in removing the difference between the π^+ and π^- best-fit radii, even though the values of these are closer to the electron scattering value than those resulting from the fits using the normal version of the code. In some cases, the best-fit radii are as much as 0.2 fm smaller when the extra potential terms are included. The fits using this modified potential seem to show a slight though probably not significant preference for an α of 500 MeV/c.

In conclusion, the angular distributions presented here exhibit an interesting structure. The failure of the first-order optical model applied in this study to adequately describe the data emphasizes the need for further studies, both experimental and theoretical, of π^+ and π^- scattering in this energy region. These will hopefully help resolve the questions raised by the present study.

ACKNOWLEDGMENTS

The authors would like to thank the LAMPF staff for their assistance during all phases of this experiment, and the Virginia Polytechnic Institute and State University machine and electronic shops for their part in construction of the wire chambers and associated electronics. We also thank W. R. Gibbs, B. F. Gibson, and G. J. Stephenson, Jr. for providing us with their optical model code, and for many detailed and useful discussions concerning the analysis of this data. This work was supported by the National Science Foundation (South Carolina and Virginia Polytechnic Institute and State University) and the Department of Energy (Los Alamos National Laboratory—through the University of California, and Oak Ridge National Laboratory—through the Union Carbide Corporation under the Department of Energy Contract fW-7405-eng-2).

---

*Present address: Los Alamos National Laboratory, Los Alamos, New Mexico 87545.

†Present address: Massachussetts Institute of Technology, Cambridge, Massachusetts 02319.

[1]D. J. Malbrough, C. W. Darden III, R. D. Edge, T. Marks, B. M. Preedom, F. E. Bertrand, T. P. Cleary, E. E. Gross, C. A. Ludeman, K. Gotow, R. L. Burman, M. A. Moinester, and R. P. Redwine, Phys. Rev. C 17, 1395 (1978).

[2]M. A. Moinester, R. L. Burman, R. P. Redwine, M. A. Yates-Williams, D. J. Malbrough, C. W. Darden III, R. D. Edge, T. Marks, S. H. Dam, B. M. Preedom, F. E. Bertrand, T. P. Cleary, E. E. Gross, C. A. Ludeman, M. Blecher, K. Gotow, D. Jenkins, and F. Milder, Phys. Rev. C 18, 2678 (1978).

[3]M. Blecher, K. Gotow, D. Jenkins, F. Milder, F. E. Bertrand, T. P. Cleary, E. E. Gross, C. A. Ludeman, M. A. Moinester R. L. Burman, M. Hamm, R. P. Redwine, M. A. Yates-Williams, S. H. Dam, C. W. Darden III, R. D. Edge, D. J. Malbrough, T. Marks, and B. M. Preedom, Phys. Rev. C 20, 1884 (1979).

[4]B. M. Preedom, S. H. Dam, C. W. Darden III, R. D. Edge, D. J. Malbrough, T. Marks, R. L. Burman, M. Hamm, M. A. Moinester, R. P. Redwine, M. A. Yates, F. E. Bertrand, T. P. Cleary, E. E. Gross, N. W. Hill, C. A. Ludeman, M. Blecher, K. Gotow, D. Jenkins, and F. Milder, Phys. Rev. C 23, 1134 (1981).

[5]B. M. Preedom, in *Proceedings of the 7th International Conference on High Energy Physics and Nuclear Structure,* edited by M. P. Locher (Birkhauser, Basel, 1977), p. 119.

[6]R. P. Redwine, in *Meson-Nuclear Physics-1979 (Houston),* Proceedings of the 2nd International Topical Conference on Meson-Nuclear Physics, edited by E. V. Hungerford III (AIP, New York, 1979), p. 501.

[7]J. Eisenberg, J. Phys. G 6, 1265 (1980).

[8]W. R. Gibbs, *Nato Advanced Study Institutes Series: Series B, Physics,* 45, edited by B. Castel, B. Goulard, and F. C. Khanna (Plenum, New York, 1979), Vol. 45, 595.

[9]R. L. Burman, R. L. Fulton, and M. Jakobson, Nucl. Instrum. Methods 131, 29 (1975).
[10]A. E. S. Green, R. J. Berkely, C. E. Watson, and C. F. Moore, Rev. Sci. Instrum. 37, 415 (1966).
[11]D. M. Lee, S. E. Sobottka, and M. A. Thiessen, Nucl. Instrum. Methods 104, 179 (1972).
[12]E. A. Wadlinger, Nucl. Instrum. Methods 134, 243 (1976).
[13]P. Y. Bertin, B. Coupat, A. Hivernat, D. B. Isabelle, J. Duclos, A. Gerard, J. Miller, J. Morgenstern, J. Picard, P. Vermin, and R. Powers, Nucl. Phys. B106, 341 (1976).
[14]W. R. Gibbs, B. F. Gibson, and G. J. Stephenson, Jr. (private communication).
[15]E. H. Auerbach, D. M. Fleming, and M. M. Sternheim, Phys. Rev. 162, 1683 (1967).
[16]W. R. Gibbs, B. F. Gibson, and G. J. Stephenson, Jr., Phys. Rev. Lett. 39, 1316 (1977).
[17]W. R. Gibbs (private communication).
[18]A. Rosenthal, Ph.D, thesis, University of Colorado, 1978 (unpublished).